Available online at www.sciencedirect.com
ScienceDirect
Journal of the European Ceramic Society 30 (2010) 2065–2072
www.elsevier.com/locate/jeurceramsoc

Effects of templating surfactant concentrations on the mesostructure of ordered mesoporous anatase TiO_2 by an evaporation-induced self-assembly method

I-Ming Hung *, Yih Wang, Cheng-Fa Huang, Yu-Shen Fan, Yi-Jhen Han, Hao-Wei Peng

Yuan Ze Fuel Cell Center/Department of Chemical Engineering and Materials Science, Yuan Ze University, No. 135, Yuan-Tung Road, Chungli, Taoyuan 320, Taiwan

Received 8 December 2009; received in revised form 16 March 2010; accepted 4 April 2010
Available online 2 May 2010

Abstract

We prepared ordered hexagonal mesoporous TiO_2 by an evaporation-induced self-assembly (EISA) method using Pluronic P123 and tetrabutyl orthotitanate ($Ti(OBu^n)_4$, TBOT) as the templating agent and the titanium source, respectively. The main purpose of this study was to elucidate the effects of surfactant concentrations on the pore arrangement, pore size, specific surface area and structure of mesoporous TiO_2 by the EISA method. The mesostructures of mesoporous TiO_2 were characterized with X-ray diffraction (XRD), nitrogen adsorption/desorption isotherms, and transmission electron microscopy (TEM). By varying the concentration of the block copolymer, mesoporous TiO_2 of various pore sizes and pore ordering were prepared. Because the mesostructure is governed by the concentration of P123 surfactant at gelation of the solution, a higher P123/TBOT mole ratio favored the formation of highly ordered mesoporous TiO_2 with a maximum pore volume of 0.26 cm^3/g, a high specific surface area of 244 m^2/g, and a BJH average pore size of 4.7 nm.

Keywords: Porosity; TiO_2; Surfactant concentration; Pore arrangement; Surface area; Evaporation-induced self-assembly method

1. Introduction

Mesoporous transition metal (TM) oxide materials, such as TiO_2, ZrO_2, Nb_2O_5, Ta_2O_5, Al_2O_3, SnO_2, WO_3, HfO_2, BN and $FePO_4$,[1–4] have gained increasing attention because of their orderly arrangement of mesopores with uniform pore sizes, high pore volumes, and specific surface area. They hold great potential in a wide range of applications such as photovoltaics,[5–7] biochemicals,[8] lithium ion batteries,[9,10] solid oxide fuel cells (SOFCs)[11,12] and sensors.[13–16] In 1995, Antonelli first reported the preparation of mesoporous TiO_2 via a sol–gel method.[17] The mesoporous structure of TiO_2 is of particular interest because the mesoporous channels offer a large surface area, and the pore wall framework is nanocrystalline, in addition, the thermal stability of mesoporous TiO_2 is better than that of traditional TiO_2 nanoparticles. This unique morphology provides a new approach for the design and fabrication of novel electrodes for high efficiency photocatalystics and photovoltaic devices.[18] Shibata reported the crystallization of mesoporous TiO_2 from an amorphous to anatase phase at calcination temperatures above 60 °C.[19] However, the collapse of the ordered mesostructure at high temperatures causes the specific surface area and thermal stability to generally decrease due to the growth of nanocrystallites in the pore walls.[20]

Ozin and co-workers produced well-defined 2D hexagonal mesoporous nanocrystalline anatase TiO_2 using P123 as the templating agent and titanium ethoxide ($Ti(OEt)_4$) as the inorganic precursor in 1-butanol solvent, replacing the ethanol commonly used in the evaporation-induced self-assembly (EISA) method.[21] During solvent evaporation, solutions become concentrated to form an ordered inorganic-surfactant mesostructure. Polymerization of the inorganic component is also simultaneously facilitated and finally the solution solidifies. Therefore, gelation before the formation of the ordered mesoporous structure must be avoided. In addition, the surfactant concentration at the moment of gelation, which is shown in Fig. 1, deter-

* Corresponding author. Tel.: +886 3 4638800x2569; fax: +886 3 4630634.
E-mail address: imhung@saturn.yzu.edu.tw (I.-M. Hung).

0955-2219/$ – see front matter © 2010 Elsevier Ltd. All rights reserved.
doi:10.1016/j.jeurceramsoc.2010.04.015

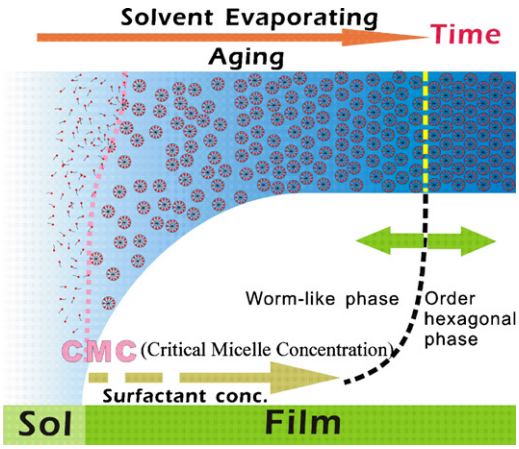

Fig. 1. Scheme of the formation of regular mesostructure micelles from surfactant molecules as solvent evaporating.

mined the structure of the residual gel. Nagamine reported that a high CTAC concentration and a low gelation rate at a low HCl concentration were favorable for the formation of highly ordered mesoporous silica and that the pore diameter increased as the CTAC/TEOS ratio increased.[22] By varying the concentration of the block copolymer, Jung reported mesoporous silica films with different pore sizes and pore orderings.[23] Xie prepared mesoporous rod-like F–N codoped TiO_2 powder using cetyltrimethyl ammonium bromide (CTAB) as a surfactant. The increasing CTAB reactive concentration extended the visible light absorption up to 600 nm.[24]

As described above, the pore arrangement of a mesoporous material strongly depends on the surfactant concentration at the moment of gelation. To our knowledge, however, the effect of the surfactant concentration on the pore arrangement, size, and surface area of mesoporous TiO_2 has rarely been reported. In the present work, we investigated the effect of the mole ratio of surfactant to titanium because it is directly related to the surfactant concentration at gelation, which is the domain factor of the highly ordered mesostructure of the mesoporous TiO_2.

2. Experimental methods

The preparation of mesoporous TiO_2 in this study was based on an evaporation-induced self-assembly (EISA) method[25] using the non-ionic amphiphilic poly(alkylene oxide) block copolymer Pluronic P123 ($EO_{20}PO_{70}EO_{20}$) (where EO is ethylene oxide and PO is propylene oxide, MW 5800, Aldrich) as the structure-directing agent and tetrabutyl orthotitanate ($Ti(OBu^n)_4$, TBOT, 99.9%, Alfa Aesar) as the titanium source. In a typical synthesis, we added 4.082 g of TBOT to 0.869–1.739 g of the P123 surfactant dissolved in 27.791 g of butanol and then added 2.912 g of 1.6 M HCl to this mixed solution with vigorous stirring at room temperature, resulting in a very acidic solution that prevented precipitation. The P123/TBOT mole ratio was in the range of 0.013–0.025. The resulting sol solution was allowed to gel in an open Petri dish as it underwent solvent evaporation at 40 RH% and 35 °C for 24 h. The as-made samples were then calcined at 350 °C for 1 h at a heating rate of 1 °C/min.

The mesostructure of samples was characterized by small angle X-ray diffraction (SAXRD) on beam line 13A at the National Synchrotron Radiation Research Center (NSRRC) in Taiwan with a wavelength λ of 1.020128844 Å. The phase identification of the mesoporous TiO_2 walls was determined using wide angle X-ray diffraction (WAXRD, XRD-6000, Shimadzu) with Ni-filtered Cu K_α radiation from 10° to 80° in 0.01° increments with a scanning rate of 4°/min. We calculated the average crystallite size of the mesoporous TiO_2 walls from the (1 0 1) peak from 20° to 30° in 0.01° increments with a scanning rate of 0.1°/min using Scherrer's equation.[26] Transmission electron microscopy (TEM) was performed using an FEI Tecnai G^2 and JEOL 2010 transmission electron microscope operating at 200 kV. The nitrogen adsorption/desorption isotherms were determined using a Micromeritics ASAP 2000 system at 77 K after the samples were vacuum dried at 200 °C overnight.

3. Results and discussion

Fig. 2 shows the N_2 adsorption/desorption isotherms of mesoporous TiO_2 prepared at different P123/TBOT mole ratios. The increase in the adsorbed volume at a relative pressure of <0.3 was due to the monolayer coverage of the surface, while the increase up to the relative pressure of 0.4–0.8 was due to the N_2 filling of the mesopores. Further increasing the relative pressure resulted in almost no increase in the adsorbed volume. All our samples showed a well-defined step in the adsorption and desorption curves between the relative partial pressures of 0.4–0.8.

Table 1
Average pore size, pore volume, specific surface area, and average crystallite size of mesoporous TiO_2 prepared at different P123/TBOT mole ratios.

P123/TBOT mole ratios	Average pore size[a] (nm)	BJH average pore size[b] (nm)	V_t[c] (cm^3/g)	S_{BET} (m^2/g)	Crystallite size[d] (nm)
0.013	3.9	3.5	0.19	169	11.1
0.015	4.3	3.9	0.22	187	10.7
0.018	4.4	4.3	0.23	206	7.5
0.020	4.9	4.7	0.26	244	8.7
0.023	4.6	5.1	0.24	247	7.8
0.025	4.8	5.3	0.20	247	12.4

[a] 4 V/A by BET.
[b] BJH adsorption average pore size.
[c] Total pore volume estimated at a relative pressure of 0.98.
[d] Average nanocrystallite size: calculated from the half-height width of the (1 0 1) diffraction peak on the WAXRD pattern using the Scherrer's equation.

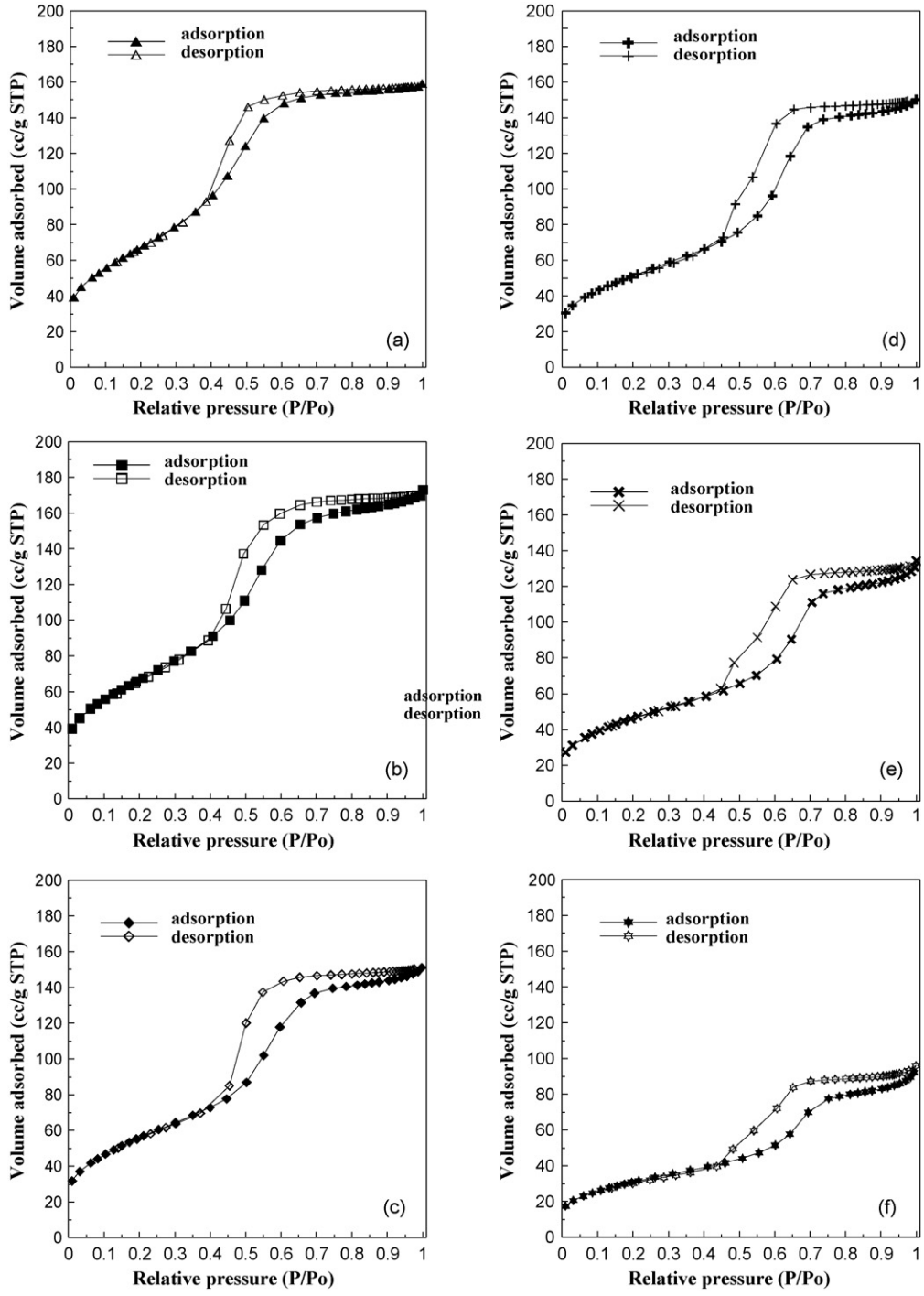

Fig. 2. N_2 adsorption–desorption isotherm curves of mesoporous TiO_2 prepared at different P123/TBOT mole ratios of (a) 0.013, (b) 0.015, (c) 0.018, (d) 0.020, (e) 0.023, and (f) 0.025.

Such adsorption behavior is typical of mesoporous materials identified as type-IV isotherms due to capillary condensation in the mesoporous channels.[27] The samples prepared at different P123/TBOT mole ratios had similar type-IV isotherms typical of mesoporous materials but different hysteresis loops. The samples prepared at P123/TBOT mole ratios from 0.013 to 0.018 showed H2 type hysteresis loops, which corresponded to their ink bottle pores. It is caused by the pore blocking from the thrust of TiO_2 nanocrystallites, a phenomenon in agreement with the TEM observation. We should note that the hysteresis loops of the samples prepared at P123/TBOT mole ratios in the range of 0.020–0.025 with their adsorption/desorption branches running parallel to each other were indicative of the H1 type, which is associated with the characteristic of cylindrical pores.

Fig. 3 shows the Barrett–Joyner–Halenda (BJH) pore-size distribution curves from the adsorption branch of mesoporous

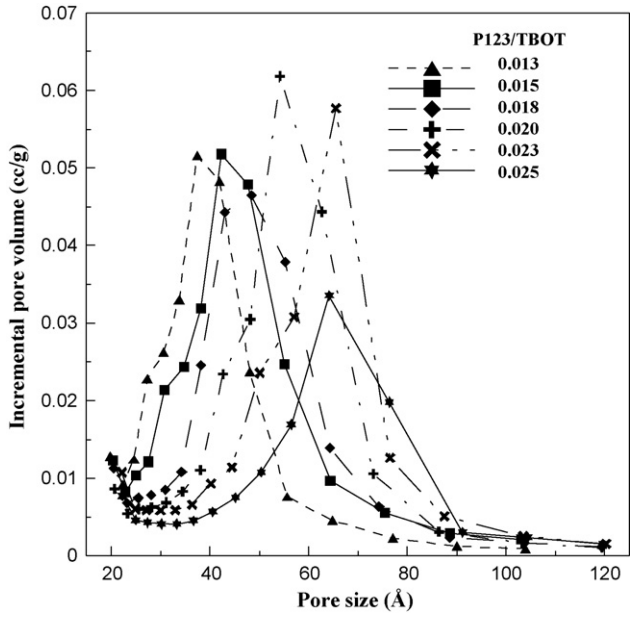

Fig. 3. BJH adsorption pore-size distribution of mesoporous TiO_2 prepared at different P123/TBOT mole ratios.

TiO_2 prepared at different P123/TBOT mole ratios in order to provide more information about the pore structure. The BJH pore sizes were in the range of 3.5–5.3 nm, and increased with the increase in the P123/TBOT mole ratio, in accordance with the structural results obtained from the SAXRD (see Fig. 4). Table 1 lists the pore sizes, pore volume, and specific surface areas of the samples with specific P123/TBOT mole ratios. Fig. 4 shows the relationship between P123/TBOT mole ratio and the BET specific surface area, pore volume, BJH average pore size and cell parameter *a* (unit cell parameter of pore arrangement which calculated from the results of the SAXRD) of the samples. The BJH average pore size and cell parameter *a* showed a linear increase with the increase in P123/TBOT mole ratio. It is well known that the micelle structure templated by the block copolymer surfactant is made up of a hydrophobic core (PPO) surrounded by hydrophilic polyethylene oxide (PEO) chains and titania walls. PEO chains form a corona region between the hydrophobic block and the titania as they dissolve into a titania framework. The charge density between titania and the block copolymer reduces during the polycondensation reaction, and the resulting PEO chains are driven into the hydrophobic region as the hydrocarbon chains elongate. Therefore, we attributed the increase in *d*-spacing in Fig. 4(a) to the elongated hydrocarbon chains caused by the increase of the P123/TBOT mole ratio.[28,29] The BET specific surface areas and pore volumes of the samples apparently increased as the P123/TBOT mole ratios increased for P123/TBOT mole

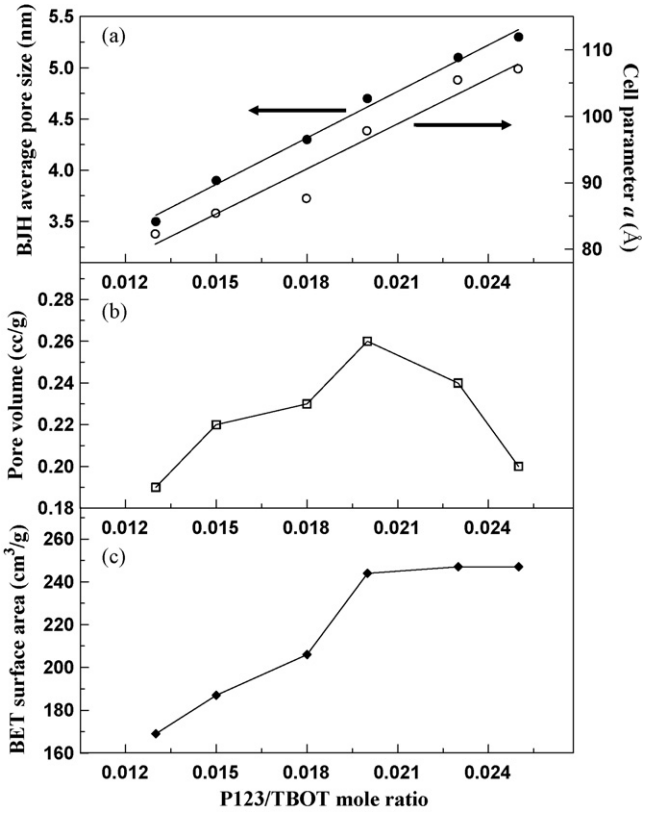

Fig. 4. Dependence of (a) BJH average pore size and cell parameter *a*, (b) pore volume, and (c) BET surface area of mesoporous TiO_2 on P123/TBOT mole ratio.

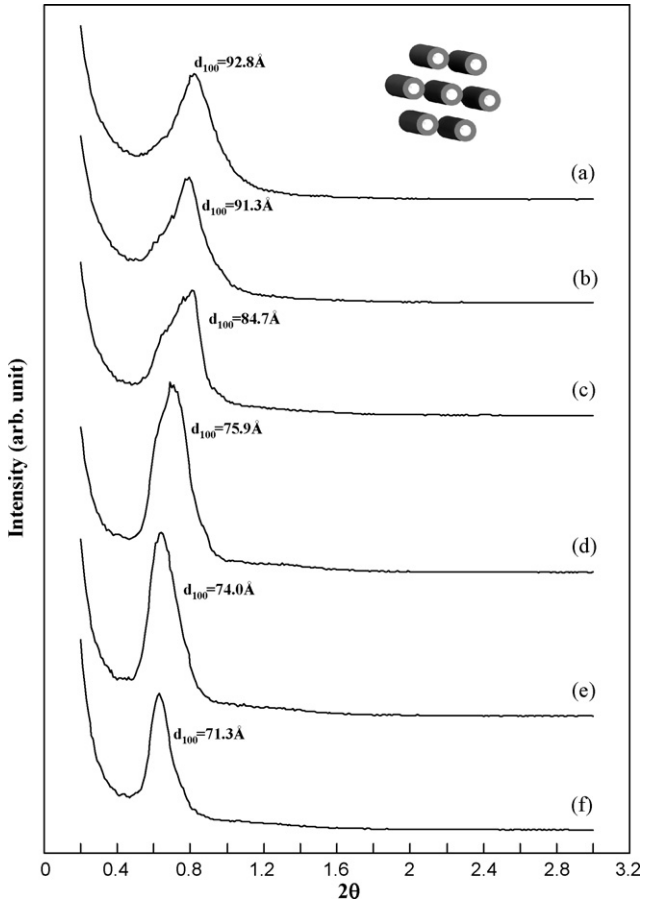

Fig. 5. Small angle X-ray diffraction patterns of mesoporous TiO_2 prepared at different P123/TBOT mole ratios of (a) 0.013, (b) 0.015, (c) 0.018, (d) 0.020, (e) 0.023, and (f) 0.025. The inset in part (a) is the schematic diagram for 2D hexagonal structure.

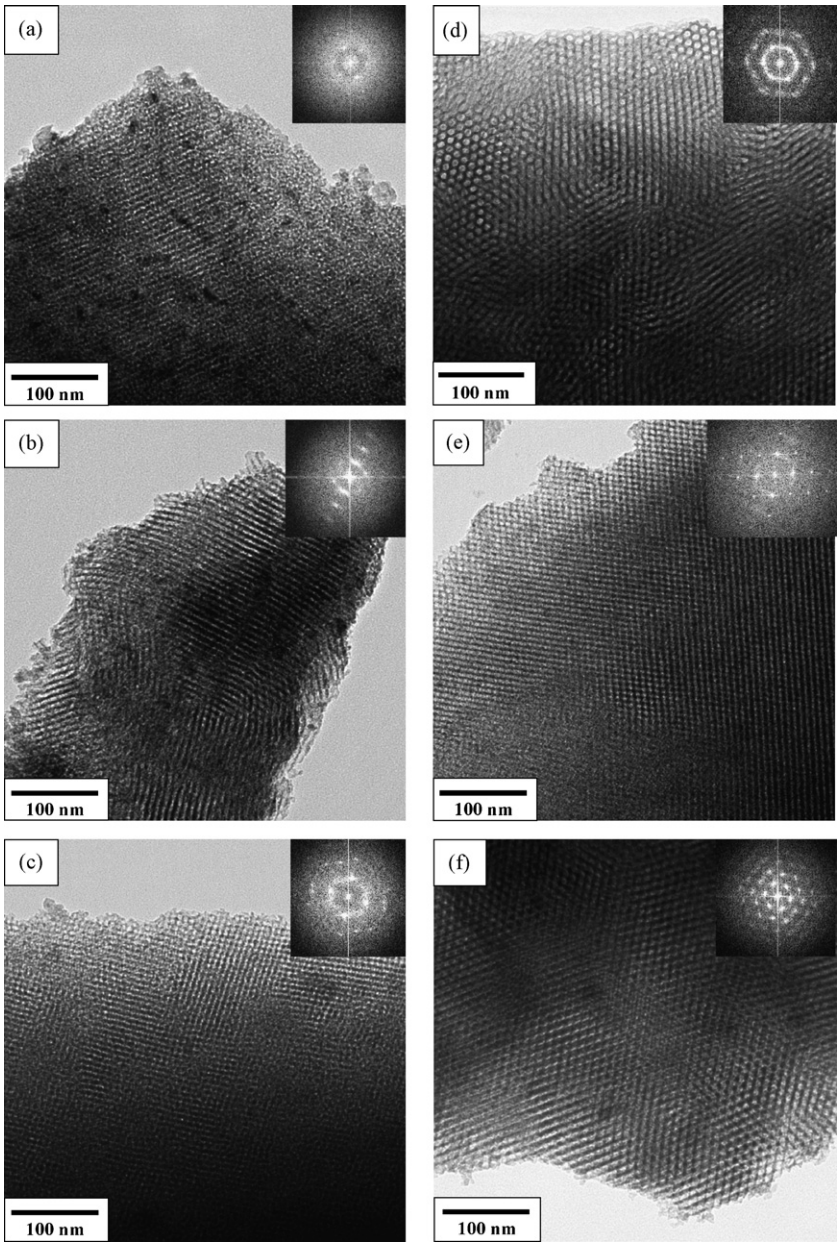

Fig. 6. TEM and fast Fourier transform (inset) images of mesoporous TiO_2 prepared at different P123/TBOT mole ratios of (a) 0.013, (b) 0.015, (c) 0.018, (d) 0.020, (e) 0.023, and (f) 0.025.

ratios in the range of 0.013–0.020. The sample prepared with a P123/TBOT mole ratio of 0.02 exhibited a maximum pore volume of 0.26 cm^3/g with a high Brunauer–Emmett–Teller (BET) specific surface area of 244 cm^3/g. Considering the large density of TiO_2 (4.2 g/cm^3), this value was commensurate with that for mesoporous silica prepared by the EISA method.[30] As the P123/TBOT mole ratio increased from 0.020 to 0.025, the BET specific surface areas of the samples remained in the range of 244 m^2/g to 247 m^2/g; however, the pore volumes of the samples apparently decreased from 0.26 cm^3/g to 0.20 cm^3/g.

The periodicity of the pore system in mesoporous TiO_2 involves repeated distances in the nanometer scale; thus, the SAXRD patterns exhibited characteristic peaks in the low angle region. Fig. 5 shows the SAXRD patterns of mesoporous TiO_2 prepared at different P123/TBOT mole ratios. The sample prepared at a P123/TBOT mole ratio of 0.013 clearly shows a main peak at 0.82°. Assuming a mesostructure with 2D hexagonal symmetry, which is expected from the replication synthesis process and confirmed by TEM images (see below), the intense diffraction peak could be indexed as the (1 0 0) reflection, corresponding to a repeat distance of $d_{100} = 71.3$ Å and a cell constant of $a = 2d_{100}/\sqrt{3}$ Å . The occurrence of the 0.82° reflection suggested that the sample might have consisted of a highly ordered structure. We found that the small angle diffraction peak of (1 0 0) shifted from 0.82° to 0.63° as the P123/TBOT mole ratio increased from 0.013 to 0.025, indicating that the d_{100} expanded from 71.3 Å to 92.8 Å, corresponding to a cell constant of $a = 107$ Å. The full width at half maximum (FWHM) of

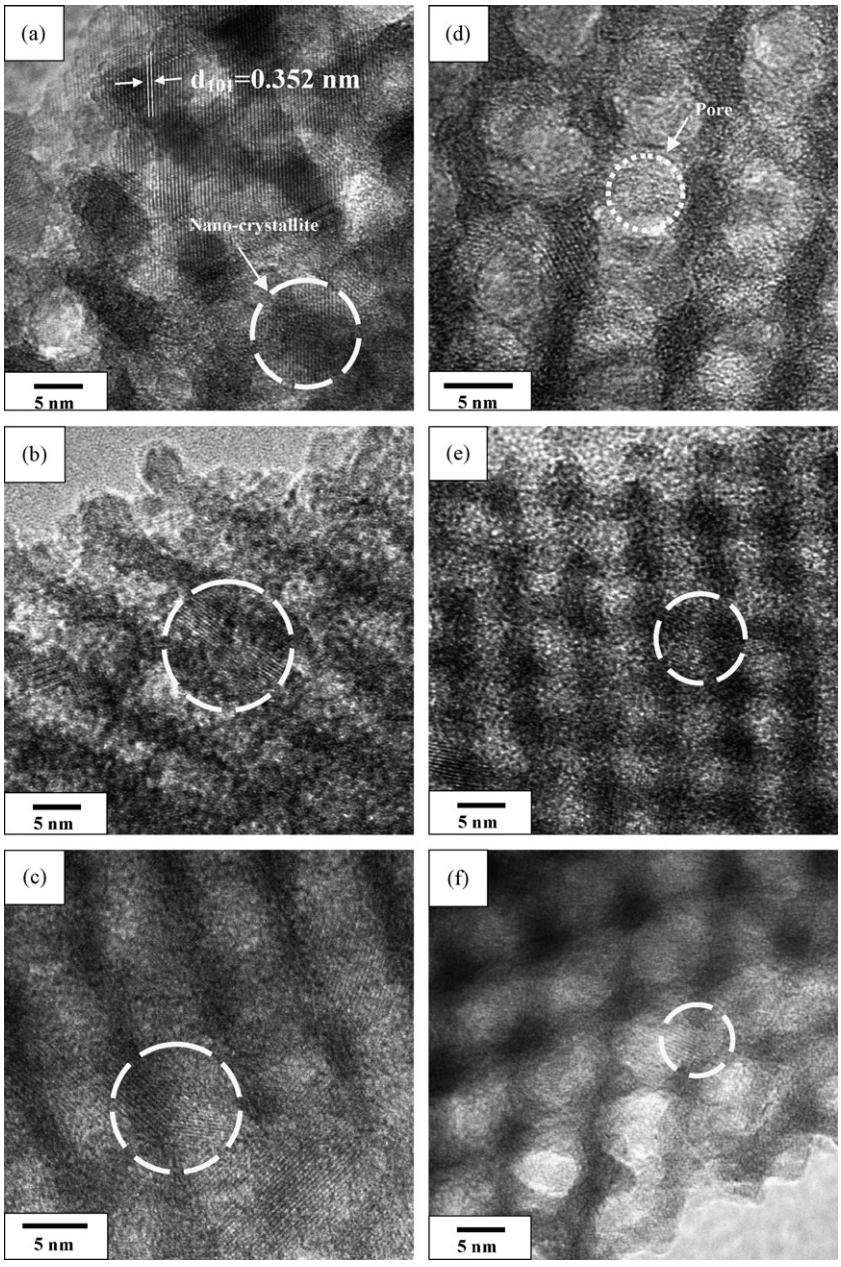

Fig. 7. HR-TEM images of mesoporous TiO_2 prepared at different P123/TBOT mole ratios of (a) 0.013, (b) 0.015, (c) 0.018, (d) 0.020, (e) 0.023, and (f) 0.025.

(1 0 0) decreased from 0.32° to 0.16° as the P123/TBOT mole ratio increased from 0.013 to 0.025, indicating that the ordering of the mesostructure increased as the P123/TBOT mole ratio increased. This result was consistent with the observations of the TEM images.

Fig. 6 shows the TEM and fast Fourier transform (FFT) images of the calcined mesoporous TiO_2 powders prepared at different P123/TBOT mole ratios. The images display highly ordered 2D hexagonal regularity in large domains, especially for the samples prepared at P123/TBOT mole ratios in the range of 0.020–0.025, a result in accordance with that of the SAXRD. These images reveal a well-defined two-dimensional hexagonal mesoporous structure along the [1 0 0] and [1 1 0] directions in the samples calcined at 350 °C from which all of the surfactant had been removed.

In order to scrutinize the microstructure and crystallization of the calcined mesoporous TiO_2, we performed high resolution TEM (HR-TEM) and WAXRD investigations as shown in Figs. 7 and 8. We clearly observed a crystallized TiO_2 framework with orderly arranged mesopores connecting in between in the sample. Numerous highly ordered pores had mean pore sizes of about 4–5 nm, and these results matched well with the BJH pore-size analyses. The lattice fringes could be clearly observed in HR-TEM images with an average *d*-spacing of about 0.350 nm, indexed as the (1 0 1) crystallographic planes of anatase and agreeing with the $d_{1\,0\,1}$ value of 0.349 nm calculated from the corresponding WAXRD patterns. HR-TEM observations further substantiated WAXRD results demonstrating the presence of the anatase phase with an average crystallite size in the range of 7–13 nm, as shown in Table 1. All the

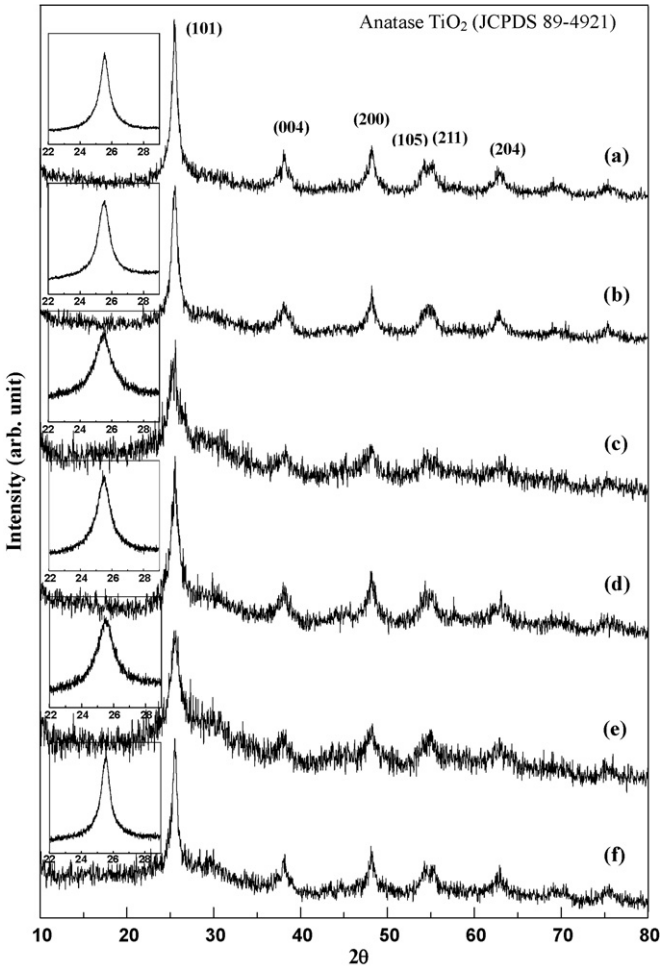

Fig. 8. Wide angle X-ray diffraction patterns of mesoporous TiO_2 prepared at different P123/TBOT mole ratios of (a) 0.013, (b) 0.015, (c) 0.018, (d) 0.020, (e) 0.023, and (f) 0.025. The inset patterns are (1 0 1) peaks from 20° to 30° in 0.01° increments with scanning rate of 0.1°/min.

samples presented distinctive peaks centered at $2\theta = 25.534°$, 38.020°, 48.102°, 53.899°, 55.023°, and 62.972° (see Fig. 8), which correspond to the anatase (1 0 1), (0 0 4), (2 0 0), (1 0 5), (2 1 1), and (2 0 4) crystalline planes (JCPDF: 89-4921), respectively. Using the width of the anatase diffraction peak and the Scherrer equation, we estimated the average crystallite sizes. The crystallite size of the samples prepared at a P123/TBOT mole ratio in the range of 0.018–0.023 is between 7.5 nm and 8.7 nm, which was smaller than those of samples prepared with both low and high concentrations of surfactant. The degradation of the mesopore ordered arrangement of the mesopores is directly related to the nanocrystalline size of the inorganic framework; as the crystal size greatly exceeds the inorganic wall thickness, the well-ordered mesostructure gradually collapses. Therefore, the samples prepared at P123/TBOT mole ratios in the range of 0.018–0.023 with smaller nanocrystallites exhibited larger pore volumes and specific surface areas with highly ordered mesostructures. The sample prepared at a P123/TBOT mole ratio of 0.025 even exhibited a high specific surface area with a highly ordered mesostructure; however, the pore volume was only 0.20 cm^3/g, possibly attributable to a large average pore size of 5.3 nm. In addition, the nanocrystallite size of the TiO_2 framework of about 12.4 nm caused the mesostructure to partly collapse to nanopowders. The results described above showed that all the samples exhibited an ordered hexagonal mesostructure. In general, a cubic or lamellar mesostructure is favorable at higher surfactant concentrations. In this case, gelation consolidated the mesostructure before the surfactant concentration became high enough to transfer from the hexagonal to cubic or lamellar phase during the solution evaporation. The degree of ordering increased with the P123/TBOT mole ratio because of the different concentrations of P123 surfactant at the moment of gelation. A higher concentration of surfactant yielded a higher degree of the ordering of the mesostructure. Notably, indicated by the shifts of SAXRD peak position to lower angles, the mesostructure of mesoporous TiO_2 expanded with the increase in the concentration of the surfactant.

4. Conclusions

We synthesized ordered mesoporous TiO_2 powders with 2D hexagonal mesostructures templated by tri-block copolymer P123 micelles by an EISA method using tetrabutyl orthotitanate ($Ti(OBu^n)_4$, TBOT) as the titanium source. Since the concentration of P123 surfactant on gelation during solution evaporation governed the mesostructure of mesoporous TiO_2, we discussed the influence of the P123/TBOT mole ratio on the mesostructure. These results showed that the P123/TBOT mole ratio governed the pore arrangement, pore size, pore volume and specific surface area of mesoporous TiO_2. A highly ordered mesoporous TiO_2 with a 2D hexagonal structure could be obtained at a high P123/TBOT mole ratio. The BJH average pore size and cell parameter a increased almost linearly with the increase in P123/TBOT mole ratio. The calcined mesoporous TiO_2 product prepared at a P123/TBOT mole ratio of 0.020 had a uniform pore size (4.7 nm), high surface area (244 m^2/g) and high pore volume (0.26 cm^3/g).

Acknowledgments

The authors acknowledge the financial support from the National Science Council in Taiwan under Contrast Nos. NSC 97-2221-E-155-059 and NSC 98-2221-E-155-068.

References

1. Yang P, Zhao D, Margolese DI, Chmelka BF, Stucky GD. Block copolymer templating syntheses of mesoporous metal oxides with large ordering lengths and semicrystalline framework. *Chem Mater* 1999;**11**:2813–26.
2. Soler-Illia GJ, de AA, Crepaldi EL, Grosso D, Sanchez C. Block copolymer-templated mesoporous oxides. *Curr Opin Colloid Interface Sci* 2003;**8**:109–26.
3. Hung IM, Hung DT, Fung KZ, Hon MH. Effect of calcination temperature on morphology of mesoporous YSZ. *J Eur Ceram Soc* 2006;**26**:2627–32.
4. Dibandjo P, Bois L, Chassagneux F, Miele P. Thermal stability of mesoporous boron nitride templated with a cationic surfactant. *J Eur Ceram Soc* 2007;**27**:313–7.
5. Coakley KM, Liu Y, McGehee MD, Frindell KL, Stucky GD. Infiltrating semiconducting polymers into self-assembled mesoporous titania films for photovoltaic applications. *Adv Funct Mater* 2003;**13**:301–6.

6. Adams WA, Bakker MG, Quickenden TI. Photovoltaic properties of ordered mesoporous silica thin film electrodes encapsulating titanium dioxide particles. *J Photochem Photobiol A: Chem* 2006;**181**:166–73.
7. Malfatti L, Falcaro P, Amenitsch H, Caramori S, Argazzi R, Bignozzi CA, et al. Mesostructured self-assembled titania films for photovoltaic applications. *Micropor Mesopor Mater* 2006;**88**:304–11.
8. Xu X, Tian B, Kong J, Zhang S, Liu B, Zhao D. Ordered mesoporous niobium oxide film: a novel matrix for assembling functional proteins for bioelectrochemical applications. *Adv Mater* 2003;**15**:1932–6.
9. Shi Z, Li Y, Ye W, Yang Y. Mesoporous $FePO_4$ with enhanced electrochemical performance as cathode materials of rechargeable lithium batteries. *Electrochem Solid State Lett* 2005;**8**:A396–399.
10. Yu A, Frech R. Mesoporous tin oxides as lithium intercalation anode materials. *J Power Sources* 2002;**104**:97–100.
11. Mamak M, Coombs N, Ozin GA. Electroactive mesoporous yttria stabilized zirconia containing platinum or nickel oxide nanoclusters: a new class of solid oxide fuel cell electrode materials. *Adv Funct Mater* 2001;**11**:59–63.
12. Wang K, Ran R, Shao Z. Methane-fuelled IT-SOFCs with facile in situ inorganic templating synthesized mesoporous $Sm_{0.2}Ce_{0.8}O_{1.9}$ as catalytic layer. *J Power Sources* 2007;**170**:251–8.
13. Innocenzi P, Martucci A, Guglielmi M, Bearzotti A, Traversa E, Pivin JC. Mesoporous silica thin films for alcohol sensors. *J Eur Ceram Soc* 2001;**21**:1985–8.
14. Teoh LG, Hung IM, Shieh J, Lai WH, Hon MH. High sensitivity semiconductor NO_2 gas sensor based on mesopporous WO_3 thin film. *Electrochem Solid State Lett* 2003;**6**:G108–111.
15. Bearzotti A, Bertolo JM, Innocenzi P, Falcaro P, Traversa E. Humidity sensors based on mesoporous silica thin films synthesized by block copolymers. *J Eur Ceram Soc* 2004;**24**:1969–72.
16. Shimizu Y, Hyodo T, Egashira M. Mesoporous semiconducting oxides for gas sensor application. *J Eur Ceram Soc* 2004;**24**:1389–98.
17. Antonelli DM, Ying YJ. Synthesis of hexagonally-packed mesoporous TiO_2 by a modified sol–gel method. *Angew Chem Int Ed Engl* 1995;**34**:2014–7.
18. Zukal MZA, Kavan L, Nazeeruddin MK, Liska P, Gratzel M. Organized mesoporous TiO_2 films exhibiting greatly enhanced performance in dye-sensitized solar cells. *Nano Lett* 2005;**5**:1789–92.
19. Shibata H, Mihara H, Mukai T, Ogura T, Kohno H, Ohkubo T, et al. Preparation and formation mechanism of mesoporous titania particles having crystalline wall. *Chem Mater* 2006;**18**:2256–60.
20. Hung IM, Fung KZ, Hung DT, Hon MH. Thermal stability of ordered mesoporous yttria-stabilized zirconia. *J Eur Ceram Soc* 2008;**28**:1161–7.
21. Choi SY, Mamak M, Coombs N, Chopra N, Ozin GA. Thermally stable two-dimensional hexagonal mesoporous nanocrystalline anatase, meso-nc-TiO_2: bulk and crack-free thin film morphologies. *Adv Funct Mater* 2004;**14**:335–44.
22. Nagamine S, Kurumada KI, Tanigaki M, Endo A. Effects of catalytic acid and templating surfactant concentrations on mesostructure of submillimeter-thick mesoporous silica by solvent evaporation synthesis. *Micropor Mesopor Mater* 2001;**49**:57–64.
23. Jung SB, Park HH. Concentration-dependent mesostructure of surfactant-templated mesoporous silica thin film. *Thin Solid Films* 2006;**494**:320–4.
24. Xie Y, Zhao X, Li Y, Zhao Q, Zhou X, Yuan Q. CTAB-assisted synthesis of mesoporous F–N-codoped TiO_2 powders with high visible-light-driven catalytic activity and adsorption capacity. *J Solid State Chem* 2008;**181**:1936–42.
25. Brinker CJ, Lu Y, Sellinger A, Fan H. Evaporation-induced self-assembly: nanostructures made easy. *Adv Mater* 1999;**11**:579–85.
26. Cullity BD. *Elements of X-ray diffraction*. California: Addison-Wesley; 1978, 284–285.
27. Gregg SJ, Sing KSW. *Adsorption surface area and porosity*. London: Academic Press; 1982.
28. Imperor-Clerc M, Davidson P, Davidson A. Existence of a microporous corona around the mesopores of silica-based SBA-15 materials templated by triblock copolymers. *J Am Chem Soc* 2000;**122**:11925–33.
29. Flodstrom K, Alfredsson V. Influence of the block length of triblock copolymers on the formation of mesoporous silica. *Micropor Mesopor Mater* 2003;**59**:167–76.
30. Dong W, Sun Y, Lee CW, Hua W, Lu X, Shi Y, et al. Controllable and repeatable synthesis of thermally stable anatase nanocrystal-silica composites with highly ordered hexagonal mesostructures. *J Am Chem Soc* 2007;**129**:13894–904.